Applied Catalysis A, General 685 (2024) 119863

Contents lists available at ScienceDirect

Applied Catalysis A, General

journal homepage: www.elsevier.com/locate/apcata

Fischer-Tropsch synthesis: Platinum promoted Co@HCS catalysts

Tshepo Molefe [a,b,c], Joy Masilo-Kumi [b], Roy P. Forbes [a,b], Neil J. Coville [a,b,*]

[a] DSI-NRF Centre of Excellence in Catalysis (c*change), South Africa
[b] The Molecular Sciences Institute, School of Chemistry, University of the Witwatersrand, Johannesburg 2050, South Africa
[c] Institute for the Development of Energy for African Sustainability (IDEAS), College of Science, Engineering and Technology, University of South Africa (UNISA), Private Bag X6 Florida 1710, Johannesburg, South Africa

ARTICLE INFO

Keywords:
Fischer Tropsch synthesis
Cobalt
Platinum
Hollow carbon spheres
Hydrogen spillover

ABSTRACT

Hollow carbon sphere (HCS) nanoreactors were used as a catalyst support for Co, with Pt as a promoter. The hollow morphology of the HCSs nanoreactor was exploited to study the influence of the Pt promoter nanoparticle location relative to that of the Co_3O_4 (Co 10 wt%) nanoparticles (d_{Co} = 3.5 – 12.5). Furthermore, the effect of Pt on the reduction behaviour and activity of the Co FTS catalyst was evaluated. The synthesis and use of Pt nanoparticles supported on/in Co@HCS FT catalysts to give CoPt@HCS and Pt/(Co@HCS) catalysts are reported. Electron microscopy, ex situ PXRD, BET, and TPR studies revealed that the prepared catalysts were successfully synthesized with well dispersed Co nanoparticles. It was observed that the proximity between the Co and Pt influenced the Co hcp/fcc ratios. A secondary hydrogen spillover effect was invoked to account for the reduction of Co_3O_4 on 1Pt/(10Co@HCS) at 335 °C. The complete reduction of Co_3O_4 to Co metal on 10Co1Pt@HCS at 350 °C was attributed to a primary hydrogen spillover effect. Following catalyst activation at 350 °C, the primary spillover process resulted in a catalyst exhibiting higher Fischer–Tropsch activity (approximately 2×) compared to both the unpromoted catalyst and catalysts where Pt and Co were separated by the HCS. This enhanced activity was partially attributed to the Co phases formed on the carbon support during reduction and the degree of catalyst reduction, which depended on the type of hydrogen spillover process. A comparison of the reduction ability of Os, Ru and Pt on the reduction of Co supported on/in HCSs and the impact of the promoter on Co hcp/fcc ratios is reported.

1. Introduction

Fischer-Tropsch synthesis (FTS) is a route for transforming non-petroleum and non-coal feedstocks, such as natural gas and biomass, into petroleum products and fine chemicals using syngas (CO/H_2) [1,2]. FTS is known to produce clean fuels (low sulphur content) and can be more economically friendly in cost compared to many other routes derived from crude oil [3,4]. Environmental problems that arise today arising from the use of crude oil, has led to a need for researchers to develop advanced and efficient catalysts to combat this issue. FTS provides one route to achieve this by utilizing non-coal carbon sources, by utilizing CO_2, and by reducing waste product formation [5,6]. Indeed, much focus on modern day FTS studies relates to the making of sustainable aviation fuels (SAFs) and the FTS process is one of the key technologies to make SAFs [7].

Cobalt catalysts dispersed on a support material are renowned for their catalytic activity and selectivity in the FTS reaction [8–10]. Co catalyst's preference for syngas conversion in FTS is due to the high intrinsic activity, high per pass conversion, good selectivity toward higher molecular weight hydrocarbons (such as SAFs) and the relatively long lifetime of a Co catalyst relative to an analogous Fe catalyst [11]. The active Co catalyst in the FTS exists as two polymorphs, the face centred cubic (fcc) and hexagonal closed packed (hcp) crystalline phases [12,13]. The catalytic activity of a Co catalyst is influenced by the relative phase abundance ratio of the Co(fcc) and Co(hcp) phases as well as the active sites that are available on the surface of the active metal catalyst [14].

Optimization of the Co catalyst FTS performance can be achieved by reactor design modification and process conditions, improving catalyst preparation methods, as well as introducing efficient support materials and promotors [15–19]. The support material interaction with the Co catalyst enhances metal dispersion and provides the anchorage to prevent catalyst sintering or agglomeration. It is known that support materials such as alumina and silica form strong metal support interactions

* Corresponding author at: DSI-NRF Centre of Excellence in Catalysis (c*change), South Africa.
E-mail address: neil.coville@wits.ac.za (N.J. Coville).

https://doi.org/10.1016/j.apcata.2024.119863
Received 20 March 2024; Received in revised form 18 June 2024; Accepted 29 June 2024
Available online 1 July 2024

(SMSI) with the Co. This results in the formation of aluminate and silicate spinel compounds which serve to anchor the metal to the support and favour high Co dispersion but at the expense of lowered reducibility. The lowered reducibility of supported Co results in a decreased number of active sites, and this reduces the effective conversion rate achievable with these catalysts.

Well-known alternative support materials that reduce SMSI effects, are carbon-based materials. Carbon materials are relatively inert and hence a moderate interaction with the metal catalyst occurs that can result in a low SMSI [20–22]. In the FTS reaction, the active catalyst (Co or Fe) has been supported on a wide variety of carbons [20]. One of these, the hollow carbon sphere (HCS) has a core-shell structure in which the core is empty. The HCSs have a high surface area, excellent electronic conductivity, low weight, are mesoporous and are relatively chemically inert. The encapsulation of active metal nanoparticles inside the HCSs has some advantages over the attachment of the metal on the outside of the shell such as i) it can restrict sintering of the metal to the metal encapsulated in the core, and ii) it can also lead to containment of any fragmented catalyst particles created during a reaction [23–25]. The hollow morphology and defective mesoporous carbon structure of HCSs thus make them an interesting carbon support for use as a Co FT catalyst. The HCSs can be used as nanoreactors for the active metal encapsulated by the carbon structure; a heterogeneous catalyst in which mass transportation of reactants (e.g., H_2 and Co) and products to/from the HCS may influence the reaction outcome [26–29]. The relative chemical inertness of HCSs also reduces the SMSI effect and enables simpler reducibility and enhanced metal catalytic activity [30,31].

Co catalyst reducibility and catalytic performance can be enhanced by an incorporation of a promoter [32]. Generally, Co promoters are noble metals (ruthenium, platinum, palladium and rhenium) that are added in small amounts to the supported Co catalyst [33]. The promoter can significantly improve the Co reducibility thus improving the Co catalyst activity, selectivity and stability [34,35]; the promoter itself may not necessarily possess catalytic activity. One of the more commonly used promoters is Pt [36,37]. Pt has a high affinity for H_2 activation (i.e. adsorption and dissociation) and is known to assist the reduction of Co oxide nanoparticles where the possibility of electronic/ligand effects from Pt-Co interactions may arise. Proposed mechanism(s) for the promotion effect(s) are linked to the promoter's location (direct or indirect contact) relative to the Co crystallites [38].

Hydrogen spillover is one of the proposed mechanisms used to explain the dissociative adsorption of a H_2 molecule in a promoted catalyst reaction [39]. Fig. 1 illustrates the two possible processes, the intrinsic primary and the secondary hydrogen spillover steps that may occur during the reduction of a Co-oxide nanoparticle in the presence of a promoter (Pt). In primary hydrogen spillover, the promoter is in direct contact with the Co-oxide and dissociation of hydrogen occurs on the promoter surface (step II) into hydrogen atoms which migrate (step III, Fig. 1(a)) to reduce Co-oxide into Co^0 (metallic) and form water (step IV, Fig. 1(a)). In secondary hydrogen spillover, the promoter and Co-oxide are separated by varying distances. Here the dissociated hydrogen atom on the promoter has to migrate on the surface of the support material (step III, Fig. 1(b)) (e.g., via hydroxyl groups on oxidic supports) followed by spillover to the Co-oxide (step IV, Fig. 1(b)) which results in the reduction of Co-oxide. This effect has been studied on numerous oxide supports, such as Co/Al_2O_3 and Pt/Al_2O_3 [40]. There have been reports of hydrogen species spilling over a distance ranging from a few nanometres to several centimetres in related Pt and Fe catalysts [41–47].

The aim of this study was to evaluate the Pt promoter effect on Co encapsulated inside a HCS (Co@HCS) catalyst during reduction experiments and FTS reactions. Two hybrid catalysts were prepared which included a bimetallic PtCo@HCS catalyst where both Pt and Co metals were encapsulated inside the HCS, and a Pt/(Co@HCS) catalyst where Co was inside, and Pt was outside the HCS. The PtCo@HCS was used to study the primary hydrogen spillover effect, while Pt/(Co@HCS) was used to study the secondary hydrogen spillover effect with the HCS carbon shell as a physical barrier between Pt and Co [50]. The HCS encapsulation ability thus enabled the study of the hydrogen spillover mechanism. Investigations were also conducted into the impact of the spillover effect on the catalysts' FT performance. Similar studies have been reported for Ru and Os promoters, and a comparison of Pt, Os and Ru as promoters in the reduction of Co on HCSs has been made [50,51].

2. Experimental

2.1. Materials

All samples were of analytical grade and were purchased from various chemical suppliers. The cobalt nitrate hexahydrate (Aldrich), hexachloroplatinic acid hexahydrate (Merck), platinum acetylacetonate [$Pt(acac)_2$, 97 %], ammonia solution (25 %; Fluka), ethanol (98 %; Merck), hexadecyltrimethylammonium bromide (CTAB; Aldrich), styrene (Aldrich), polyvinylpyrollidone (PVP, MW 40 K, Aldrich), formaldehyde (37 %; Aldrich), potassium persulfate (Eimer and Amend), hydrazine (35 % Aldrich), and deionized water were used as received for the experiments.

2.2. Synthesis of Co@HCS and CoPt@HCS catalysts

2.2.1. The synthesis of polystyrene spheres (PSSs)

Styrene (8 mL) and polyvinylpyrollidone (PVP, 0.2 g) was dispersed and dissolved in a mixture of 200 mL ethanol and 50 mL deionized water in a round bottom flask using a previously reported synthesis method [51]. The mixture was sonicated and stirred for 15 min. Thereafter, potassium persulfate (KPS, 0.3 g in 10 mL deionized water) was added to the prepared reaction mixture while stirring. The mixture was then heated at 80 °C for 24 h. After the reaction the product was cooled, filtered, and washed successively using deionized water. The obtained yield was ~ 6 g.

2.2.2. Synthesis of Co or CoPt on the polystyrene spheres (10Co/PSSs; 10CoxPt/PSSs) (x = 0.1, 0.5, 1)

PSSs (3 g) were added to a mixture of 75 mL deionized water and 25 mL ethanol. Cobalt nitrate hexahydrate (0.45 g) was added to this

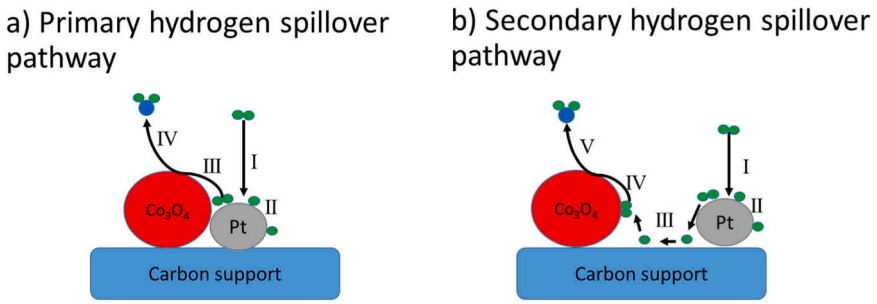

Fig. 1. (a) Primary and (b) secondary hydrogen spillover mechanism (pathways) [48,49].

mixture while stirring, until the solution turned red. Thereafter, 10 mL of hydrazine (2 M) was slowly added to the prepared solution dropwise, and the solution was stirred for 12 h to ensure the complete deposition of the Co nanoparticles onto the PSSs. The sample was called 10Co/PSS [52].

The bimetallic CoPt/PSSs composite was prepared by adding both the cobalt (0.45 g) precursor and the ammonium hexachloroplatinic acid hexahydrate (0.05 M, 3 mL) onto the PSS, followed by hydrazine addition as stated above. This was expected to give a catalyst with a nominal Co/Pt mol ratio of 10:1. The sample was called 10Co1Pt/PSS. Two further catalysts with mol ratios of Co:Pt of 20:1 and 100:1 (10Co0.5Pt/PSS and 10Co0.1Pt/PSS) were made by the same method as above but using, 1.5 mL and 0.3 mL of ammonium hexachloroplatinic acid hexahydrate (0.05 M), respectively. Yields of > 90 % were obtained.

2.2.3. Synthesis of Co or CoPt nanoparticles encapsulated inside hollow carbon spheres (10Co@HCS and 10CoxPt@HCS)

The catalysts 10Co/PSSs or 10Co1Pt/PSSs (1 g) and ammonia solution (25 %; 4 mL) were added to a mixture of 70 mL ethanol and 15 mL deionized water and the mixture was sonicated for 30 min. Subsequently, resorcinol (0.5 g), formaldehyde (0.5 mL) and hexadecyltrimethylammonium bromide (3 g) were added to the above solution. The solution was allowed to stir at room temperature for 24 h. A resorcinol-formaldehyde (RF) core shell structure formed around the 10Co/PSSs or 10Co1Pt/PSSs and the material was filtered and washed successively with water and ethanol, followed by drying at 80 °C for 12 h. Template removal and carbonization of the prepared composites was performed using a two-step horizontal chemical vapour deposition procedure. Template removal was done under a flow of nitrogen gas (50 mL/min) at an isothermal temperature of 350 °C for 1 h to decompose and remove the PSSs. This was followed by carbonization of the RF core shell structure under a flow of nitrogen gas (50 mL/min) at 600 °C for 2 h. The resulting products were called 10Co@HCS and 10Co1Pt@HCS. The same method was used to make 10Co0.5Pt/PSS and 10Co0.1Pt/PSS samples to give the catalysts 10Co0.5Pt@HCS and 10Co0.1Pt@HCS. Yields of > 90 % were obtained.

2.3. Synthesis of xPt/(Co@HCS) (x = 0.1, 0.5, 1) catalyst

To achieve a nominal 1 wt% loading of Pt onto the surface of a 10Co@HCS catalyst (containing 10 wt%Co), platinum acetylacetonate [$Pt(acac)_2$, 97 %] (13.5 mg) was added to the 10Co@HCS (0.4 g) catalyst and this was sonicated for 10 min to thoroughly dry-mix the two solids. The mixed composite was then transferred into a cylindrical quartz tube that was placed in a tubular horizontal furnace under a steady argon (50 mL/min) stream. The furnace was ramped to 100 °C and kept isothermal for 30 min to remove any moisture from the sample. The furnace was further ramped up to 350 °C at a heating rate of 2.5 °C/min and kept isothermal for 2 h. After 2 h, the reactor was left to cool down to room temperature to produce 1Pt/(10Co@HCS) [53].

For the 0.5Pt/(10Co@HCS) and 0.1Pt/(10Co@HCS) products, the same method as above was used, but with 6.75 mg and 1.35 mg of platinum acetylacetonate [Pt(acac)2, 97 %] respectively.

2.4. Catalyst characterization

TEM analysis was performed on a Tecnai spirit (T12) transmission electron microscope operating at 120 kV. The samples were dispersed in methanol by ultra-sonication and loaded onto a copper grid for TEM analysis. The particle size distribution of the materials formed was determined by counting at least 200 randomly selected particles per sample from different TEM images. Gaussian statistics yielded values for the average particle sizes. SEM analysis was performed on a FEI Nova Nanolab 600 FIB/SEM instrument operating at 30 kV. The samples were collected on a carbon tape and were coated with a gold−palladium layer prior to analysis. The bulk crystalline phase composition of the catalysts was studied using a Bruker D2 Phaser powder X-ray diffractometer equipped with a Co−Kα X-ray source (λ = 1.7889 Å), a flat plate sample stage and a Lynxeye PSD detector. The scan range was from 10° to 90° 2θ in 0.0260°.

N_2 adsorption−desorption experiments were conducted at −195 °C using a Micromeritics Tristar 3000 surface area and porosity analyser. Prior to an experiment, the sample was outgassed at 150 °C for 4 h under N_2 gas. The BET surface areas were obtained from adsorption data in a relative pressure range from 0.05 to 0.30. The total pore volumes were calculated from the amount of N_2 vapour adsorbed at a relative pressure of 0.99. The pore size distributions were evaluated from the desorption branches of the isotherms using the Barrett−Joyner−Halenda (BJH) method. The micropore surface area and volume were calculated using t-plot data.

TPR experiments were carried out with a Micromeritics Auto Chem II unit. The catalyst (approximately 50 mg) was placed in a tubular quartz reactor, fitted with a thermocouple for continuous temperature measurement. The reactor was heated in a furnace. Prior to the temperature-programmed reduction measurement, the calcined catalysts were flushed with high purity Ar gas at 200 °C for 30 min, to remove water and impurities, followed by cooling to ambient temperature. Then, the gas supply was switched to 5 % H_2/Ar, and the temperature was raised at a rate of 10 °C min^{-1} from 50 to 850 °C. The gas flow rate through the reactor was controlled by three Brooks mass flow controllers and was kept constant at 50 mL.min^{-1}. The H_2 consumption (TCD signal) was recorded automatically. Pulse chemisorption was performed using the Micromeritics Auto Chem II instrument, to compute the number of active sites on the catalysts. The catalyst (ca. 100 mg) was placed in a tubular quartz reactor. The sample was reduced at 350 °C for 2 h under a H_2 flow of 50 mL.min^{-1}. Before injection of the active gas, the sample was purged using helium gas at 350 °C for 1 h, followed by cooling to ambient conditions.

2.5. Data Reduction and Interpretation

For all PXRD data presented, the crystalline phase identification was done using DIFFRAC.EVA (Version 4.2. Release 2016) using the crystallography open database (COD) (Release 2020). Phase analysis was done using the Rietveld method as implemented in Bruker AXS TOPAS software (Version 5, 2014). HCS diameter and carbon shell thickness were determined using TEM images and ImageJ software (1.48 version).

2.6. Fischer-Tropsch synthesis catalyst evaluation

The FTS reaction was performed in a fixed-bed micro-reactor. A gas cylinder containing a $H_2/CO/N_2$ mixture (~60/30/10 vol%; purity 99.99 %) was used to supply the reactant gas stream to the catalyst with a specific space velocity of 1800 mL h^{-1} g^{-1}. N_2 was used as an internal standard in order to ensure accurate mass balances. Catalyst (0.5 g, sieved through a 150 μm mesh, without pelletizing) was added to the reactor (resulting catalyst bed ~4 cm in length) and reduced in situ at 350 °C for 2 h under a stream of H_2 (1.5 bar at 50 mL.min^{-1}). After reduction, the reactor temperature was decreased to ambient temperature under a hydrogen flow and then heated up to 220 °C under synthesis gas at a pressure of 10 bar. A hot trap placed immediately after the reactor was held at 150 °C in order to collect wax. A second trap kept at ambient temperature was used to collect the oil and water mixture. All gas lines after the reactor were kept at 100 °C. The flow was controlled using a metering valve and measured by a bubble meter. The product stream was analysed online using two gas chromatographs. A thermal conductivity detector (TCD), equipped with a Porapak Q (1.50 m × 3 mm) packed column, was used to analyse H_2, N_2, and CO, and a flame ionization detector (FID), equipped with a Porapak Q packed column, was used for the analysis of the hydrocarbons online using the Clarity software package.

3. Results

3.1. Transmission electron microscopy (TEM)

The synthesis of the hollow carbon spheres (HCSs) was achieved by using monodispersed polystyrene spheres (PSSs) as a template using a standard procedure [54]. A TEM image of the PSSs showed that they were uniform, spherical in shape, and had a smooth surface (Fig S1 (a)). The particle size distribution was between 350 and 600 nm with an average diameter of 490 nm (Fig S1 (b)). The PSSs were prepared to be larger than 200 nm in diameter to prevent both coagulation from occurring as well as the formation of large, connected nanospheres [55]. The PSS template was then coated with Co (10 wt%) and Pt (0.1, 0.5 and 1 wt%) to form 10Co/PSSs or 10CoxPt/PSSs (x = 0.1, 0.5, 1 wt%).

The 10Co/PSSs or 10Co1Pt/PSSs template was then covered with RF (resorcinol formaldehyde) and CTAB. It was important for the carbon shell of the support to be porous with short dimensions to enable both primary and secondary hydrogen spillover to take place. This was achieved by the addition of CTAB. The addition and RF polymerization steps led to the Co/PSS coating as previously reported [56,57]. The synthesized RF coated template was then heated to decompose the PSS template and carbonization took place to form the 10Co@HCS or 10Co1Pt@HCS. The same method was used to convert the RF covered 10Co0.5Pt/PSS and 10Co0.1Pt/PSS prepared samples, to give the products 10Co0.5Pt@HCS and 10Co0.1Pt@HCS.

Fig S2 shows the TEM images of the (a) HCS support and (b) their shell thickness. The HCS diameter ranged from 350 to 400 nm with the average size of 380 nm and the carbon shell thickness had an average width of 28 ± 5 nm. The average HCS diameter (380 nm) was lower than that of the polystyrene spheres (495 nm) and this was due to a shrinkage that occurs during the carbonization process [58], as well as dehydration of the cross-linked carbon precursor that occurs during carbonization [59,60].

Electron microscopy measurements were performed to verify the architectures of the synthesised Co catalysts (Fig. 2). The synthesised Co@HCS catalyst had well dispersed Co nanoparticles (3.5 ± 2 nm) inside the HCS support (Fig S3). The TEM images, Fig. 2, revealed a spherical HCS morphology with metal nanoparticles in the core shell structure for the bimetallic PtCo@HCS catalysts (Fig. 2a, b, and c) and a similar morphology for the Pt/(Co@HCS) catalysts (Fig. 2d, e, and f). TEM images of the catalysts revealed that the majority (> 90 %) of the HCS's support structure was still intact and undamaged. [24,61].

The Co@HCS catalyst (no Pt) had an average Co particle size of 3.5 ± 1 nm [51]. The average size of the Co nanoparticles in (a) 10Co0.1Pt@HCS, (b) 10Co0.5Pt@HCS, and (c) 1 % Pt/10 %Co@HCS catalysts were 5 ± 3 nm, 6 ± 3 nm and 7 ± 2 nm, respectively. The Co size also increased for the Pt/(Co@HCS) catalysts. The average particle size of the Co nanoparticles in catalysts (d) 0.1Pt/(10Co@HCS), (e) 0.5Pt/(10Co@HCS), and (f) 1Pt/(10Co@HCS) were 5 ± 3 nm, 6 ± 2 nm and 6 ± 3 nm, respectively. A similar trend was observed in a study where the effects of Co and Ru intimacy in FTS catalysts was investigated using HCS supports where it was found that the Co change in particle size was insignificant with the introduction of a Ru promoter [50]. In contrast, the introduction of an Os promoter showed a change in the particle size of Co in relation to intimacy in CoOs@HCS catalysts, and as the Os percentage loading increased [51].

In contrast, Zhang et al. reported that a Pt promoter added to Co catalyst, supported on carbon nanotubes, produced no noticeable increase in the size of the Co nanoparticles. The small size effect observed was attributed to a chemical interaction between the Co-oxide nanoparticles and the support resulting from the decomposition of the Co precursor on the support [62]. Chu et al. also confirmed that no significant effect was observed from adding Pt to Co_3O_4 nanoparticles supported on Al_2O_3 and attributed the size of the Co_3O_4 nanoparticles to the pore diameter of the support [63].

The Pt nanoparticles in the xPt/(10Co@HCS) were difficult to observe due to their low loadings and the carbon shell thickness, and little can be said about their size from the TEM images recorded [64].

3.2. Scanning electron microscopy (SEM) and energy dispersive X-ray (EDX) spectroscopy analysis

The synthesised catalysts were confirmed to be spherical and hollow in structure, as confirmed from the SEM images of non-broken HCS's,

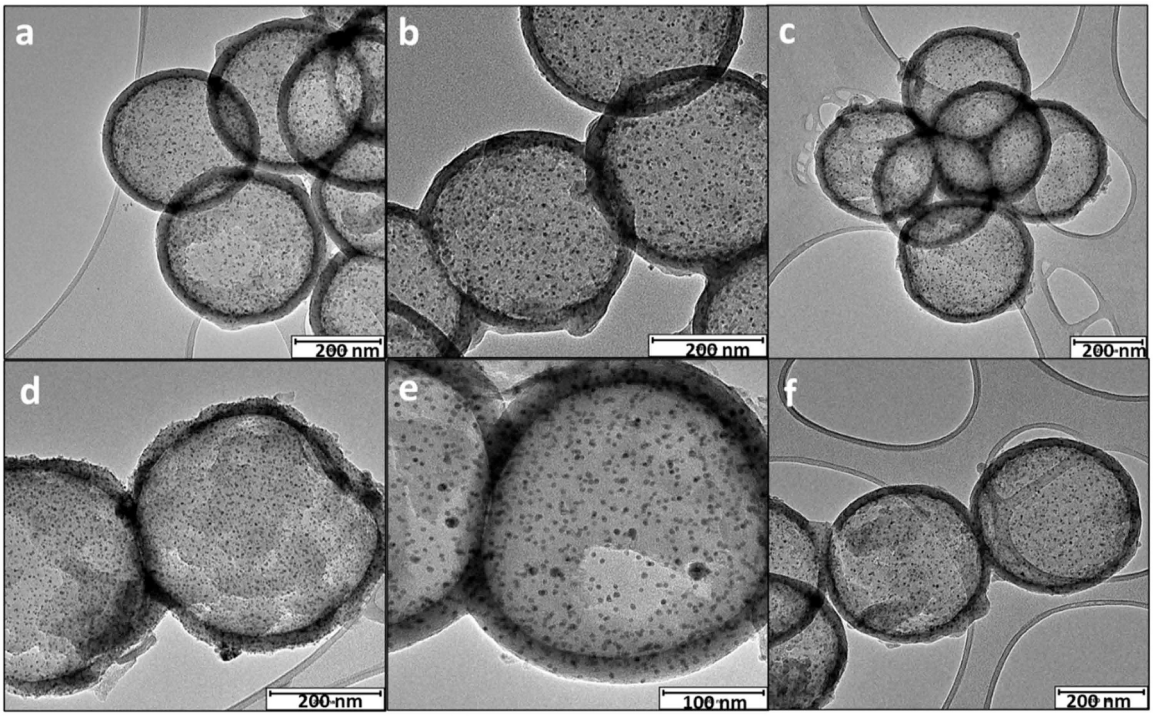

Fig. 2. TEM images of (a) 10Co0.1Pt@HCS, (b) 10Co0.5Pt@HCS, (c) 10Co1Pt@HCS, (d) 0.1Pt/(10Co@HCS), (e) 0.5Pt/(10Co@HCS), and (f) 1Pt/(10Co@HCS).

and some partially broken HCSs. The EDX analysis also showed the elemental composition of the synthesized nanostructure catalysts. Thus, Fig. S4 (a), Fig S5 (a) and Fig S6 (a) shows the SEM images of 10Co@HCS, 1Pt/10Co@HCS, and 1Pt/(10Co@HCS) respectively. From EDX spectrum 1 (Fig. S4 (b)) it can be confirmed that Co nanoparticles were indeed present in Co@HCS, and both Co and Pt nanoparticles were present in the Pt/Co@HCS and Pt/(Co@HCS) catalysts (Fig S5 (b) and S6 (b)). The other Pt (0.5 % and 0.1 %) loaded catalysts showed similar results.

3.3. Powder X-ray diffraction (PXRD)

PXRD patterns of 10Co@HCS, Pt/10Co@HCS and Pt/(10Co@HCS) catalysts are shown in Fig 5.3 (a) and (b). The broad peak at 2θ between 25° and 30° observed for all the synthesised catalysts was attributed to the structure of the disorderd sp^2 hybridized carbon shell [65]. Due to the very small quantities (loadings) of the Pt promoter, its small particle size and its even dispersion, the diffraction pattern of Pt metal was not observed in the PXRD data.

The various PXRD diffraction patterns for the Co and Co/Pt catalysts showed the presence of Co_3O_4, CoO and the Co(fcc) and Co(hcp) phases (Fig. 3, Table 1 and S1). A comparison of the patterns of the synthesised catalysts showed that the peaks observed in the data were due to both the Co_3O_4 and CoO phases (ICSD: 9362 and COD: 9008618, respectively). The presence of the CoO phase was due to the autoreduction of the Co_3O_4 phase when it was in contact with the carbon shell. This type of autoreduction process was also previously observed for Co@HCS catalysts promoted by Os [51,66].

The Co(fcc) and Co(hcp) phases were present in the Pt promoted catalysts (Table 1) and the peaks due to these phases increased with an increase in Pt loading. The data suggests that Pt (and carbon) promoted the reduction of Co oxides, with no significant Co particle size change (see TEM data). The 10CoxPt@HCS catalysts Co showed an increase in the Co hcp/fcc ratios that followed the pattern: 10Co0.1Pt@HCS (0.19) < 10Co0.5Pt@HCS (0.23) < 10Co1Pt@HCS (0.75) suggesting that the Pt induced an increase in the hcp Co content. In contrast, the 10CoxPt@HCS catalysts had Co hcp/fcc ratios that followed the pattern: 0.1Pt/(10Co@HCS) (n/a) > 0.5Pt/(10Co@HCS) (0.60) > 1Pt/(10Co@HCS) (0.52) suggesting that when the Pt was physically removed from the Co, the hcp ratio did not increase. In summary, the comparison of the Co (hcp/fcc) ratios for the 10CoxPt@HCS and xPt/(10Co@HCS) catayst showed that an increase in Pt loading in the 10CoxPt@HCS catalysts gave more hcp Co than in the xPt/(10Co@HCS) catalysts. The data is consistent with the literature which has indicated that low reduction temperatures usually leads to the formation of Co (hcp) while a high reduction temperatures leads to Co (fcc) formation [40]. The Co (hcp) phase has been reported in the literature to be the more active phase than the Co (fcc) phase in the FT reaction. This data suggests that the one of the roles played by the Pt promoter is to enhance the formation of the Co (hcp) phase for the FT process [67].

Similar effects have been reported for a Ru-Co system to elucidate Ru promoter effects [68,69]. For example, Hong et al. utilized X-ray spectroscopy (XAS) and found that a Co_3O_4 nanoparticle lattice containing implanted Ru ions served as a promoter for Co_3O_4 reduction at low temperatures [32]. Similar observations have demonstrated that the close proximity of an Os promoter to Co improved the reducibility of Co_3O_4 nanoparticles, influencing the Co phase in the presence of the Os promoter nanoparticle [51].

3.4. Nitrogen absorption-desorption analysis

Textural properties of the HCSs and prepared catalysts was analysed using the nitrogen absorption-desorption method (BET). Fig S7, illustrates the N_2 absorption-desorption isotherm curves of the HCS and the Co@HCS, CoxPt@HCS and xPt/(Co@HCS) catalysts. All the catalysts presented the type I/IV adsorption isotherms which reveal both micropores and mesopores [69].

Table 2 shows the data collected for the surface area, pore volume and pore size for HCSs of the prepared catalysts. The porous nature of the HCS carbon shell was enhanced by the porogen (CTAB) that was used during the carbon shell synthesis [70]. A similar observation of high surface area and microporosity of HCS materials has been reported as a result of using other microporous spherical templates [24,71]. The surface area of the HCSs was shown to decrease with the introduction of metals loaded inside or outside the HCS support material, and this can be accounted for by the metal nanoparticles covering some of the micropores, thus altering the carbon shell's pore structure.

3.5. Temperature programmed reduction (TPR)

A TPR study was conducted to determine the Co reduction behaviour and the impact of the Pt promotor on the synthesized catalysts. Data is shown in Fig S8. Peaks above 600 °C for catalysts supported on carbon materials are usually assigned to the gasification of the carbon support

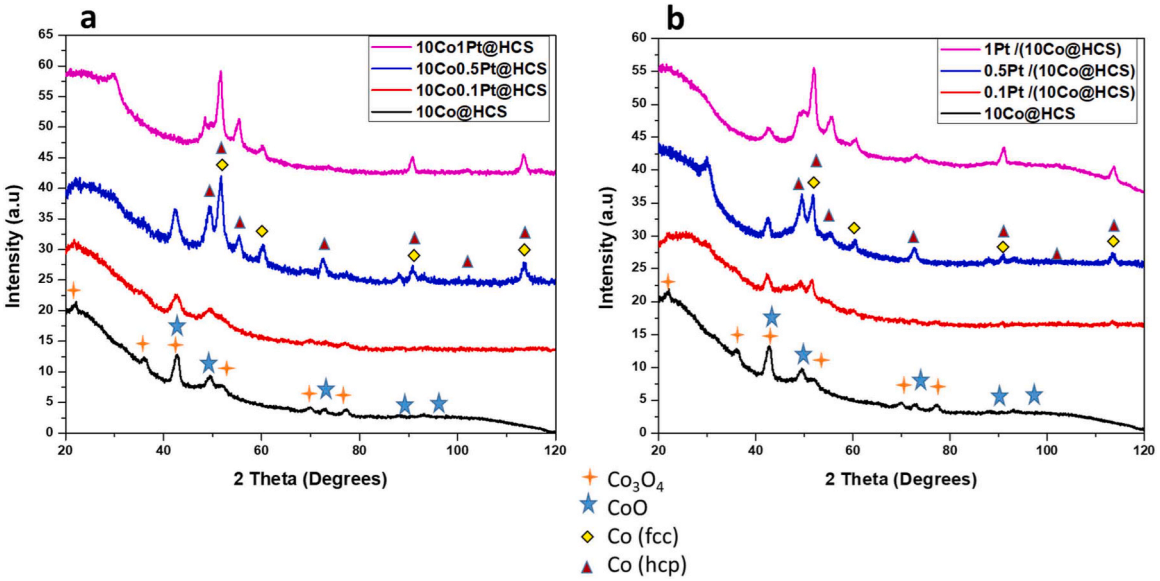

Fig. 3. PXRD pattern of (a) Pt/Co@HCS and (b) Pt/(Co@HCS) catalysts.Co@HCS patterns are also shown for comparison.

Table 1
Relative Co phase abundances (wt%).

SAMPLE	Co_3O_4	CoO	Co(fcc)	Co(hcp)	Other	Hcp/fcc ratio
10 %Co@HCS	56.554	43.45	-	-	-	-
10Co0.1Pt@HCS	-	63.24	30.96	5.81	-	0.19
10Co0.5Pt@HCS	-	55.87	35.92	8.21	-	0.23
10Co1Pt@HCS	-	31.37	39.206	29.43	-	0.75
0.1Pt/Co@HCS	**Not enough useable information in XRD data info**	n/a				
0.5Pt/(10Co@HCS)	-	17.83	20.78	12.49	**Graphite** 48.90	0.60
1Pt/(10Co@HCS)	-	5.83	31.18	16.09	**Graphite** 46.89	0.52

Table 2
Textural properties (surface area, pore volume and average pore size) of the hollow carbon sphere support and the Co encapsulated catalysts.

Sample	Surface Area (m^2/g)	Pore Volume (cm^3/g)	Mesopore Size (nm)
HCSs	532	0.51	5.0
10Co@ HCS	508	0.59	9.8
10Co0.1Pt@HCS	371	0.54	8.7
10Co0.5Pt@HCS	358	0.63	6.8
10Co1Pt@HCS	323	0.21	3.1
0.1Pt/(10Co@HCS)	495	0.73	6.9
0.5Pt/(10Co@HCS)	435	0.67	5.4
1Pt/(10Co@HCS)	389	0.48	4.2

when using CNTs [3,57] and solid carbon spheres [18].

To observe the Co reduction peaks, the TPR profiles were expanded in the region < 500 °C (Fig. 4 and Fig. 5). All of the catalysts showed a peak at temperatures below 150 °C and this peak is attributed to the evolution of water. Although not expected, it is also possible that the peak could be due to NOx species due to the reduction of nitrate species, remnants of the $Co(NO_3)_2$ precursor or even to the reduction of CoOOH species to Co_3O_4 [72].

The TPR behaviour exhibited the typical two-step reduction of Co_3O_4 species via conversion to a CoO intermediate phase with the final step being the conversion of CoO to metallic Co [73] viz.

First reduction step: $Co_3O_4 + H_2 \rightarrow 3CoO + H_2O$ (ca. 230 – 320 °C) (1)

Second reduction step: $3CoO + 3H_2 \rightarrow 3Co + 3\,H_2O$ (ca. 325 – 430 °C) (2)

The first reduction and second reduction peaks in the TPR are shown in Table 3. The unpromoted Co@HCS catalyst had reduction peaks at 320 °C, and at 430 °C. The reduction temperature of both the first and second reduction peaks was decreased in the presence of Pt [62,74]. The extent of the downward shift of the reduction peak to lower temperatures was influenced by the relative locations of the Pt and Co.

The TPR profiles of the (0.1, 0.5 and 1 % Pt loading), and 10 % Co@HCS catalysts are shown in Fig. 4(a). As can be seen from the intensity of all the Pt promoted Co samples, the peaks are small due to partial reduction that occurred during the synthesis stages when Co was close to Pt. The addition of Pt had an effect on both the reduction steps; this is in agreement with reports in the literature on the effect of Pt on Co reducibility [62]. The change in temperature for the first reduction step of Co_3O_4 was approximately by 5, 58 and 95 °C for the CoxPt@HCS catalysts (x = 0.1 %, 0.5 %, 1 %, respectively), Fig. 4(b). The second reduction step showed a larger change in the reduction temperature with Pt percentage loading, with changes of approximately 40, 108 and 79 °C for the three xOsCo CoxPt@HCS catalysts. This observation is in agreement with a study on co-impregnation of SiO_2 and Al_2O_3 with Co $(NO_3)_2{\cdot}6\,H_2O$ and $Pt(NH_3)_4(NO_3)_2$ which revealed a significant enhancement in the reduction of Co oxide [75].

The TPR profiles of the Pt/(10Co@HCS), (0.1, 0.5 and 1 % Pt loading) and the 10 % Co@HCS catalysts are shown in Fig. 5(a). It is noted that when a higher percentage loading of Pt is added to the Co@HCS, Fig. 5(b), a downward shift of the reduction peaks, relative to the reduction step of Co@HCS, occurred (Fig. 5(b)). As the percentage loading increased the change in the first reduction step temperature was approximately 5, 52, 70 °C for the three Pt promoted catalysts, xPt/(Co@HCS) (x = 0.1 %, 0.5 % and 1 %, respectively). The second reduction step temperature change also showed changes (20, 34, 98 °C, respectively). This downward shift to lower temperature of the reduction peaks is due to a secondary spillover effect involving the carbon shell that separates the Co_x and Pt, acting as a physical barrier that allows diffusion of H atoms between the Pt and Co. The apparent decrease in the amount of hydrogen uptake also suggested the occurrence of diffusion limitations of the H atoms when the Co-oxide is separated from the Pt [38]. This secondary hydrogen spillover effect has been observed, in Pt-Co [76] and Rh-Co [77] catalysts supported on alumina, and with Ru-Co and Os -Co catalysts supported on HCSs [50,51].

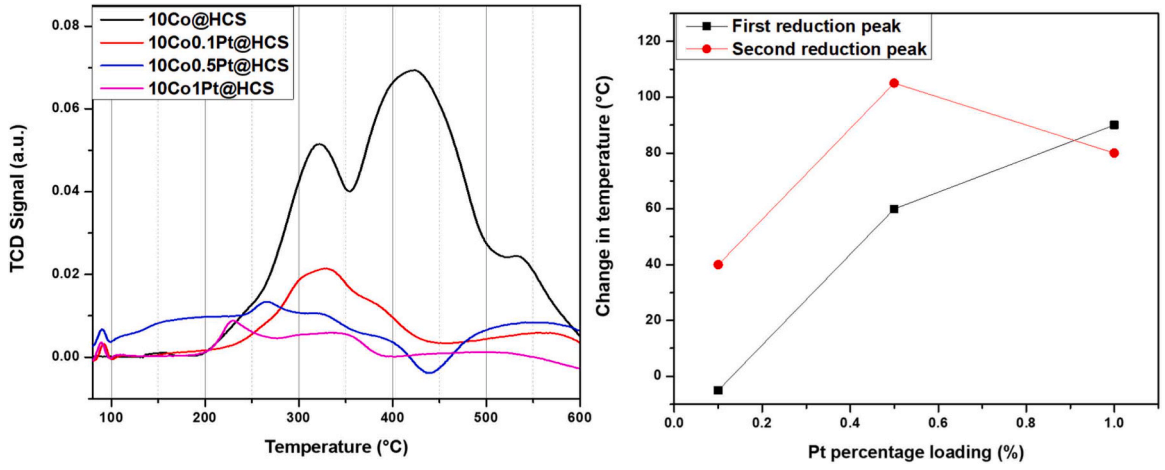

Fig. 4. (a) TPR profile of the 10CoxPt@HCS catalysts and (b) the relative change in temperature with Pt percentage loading.

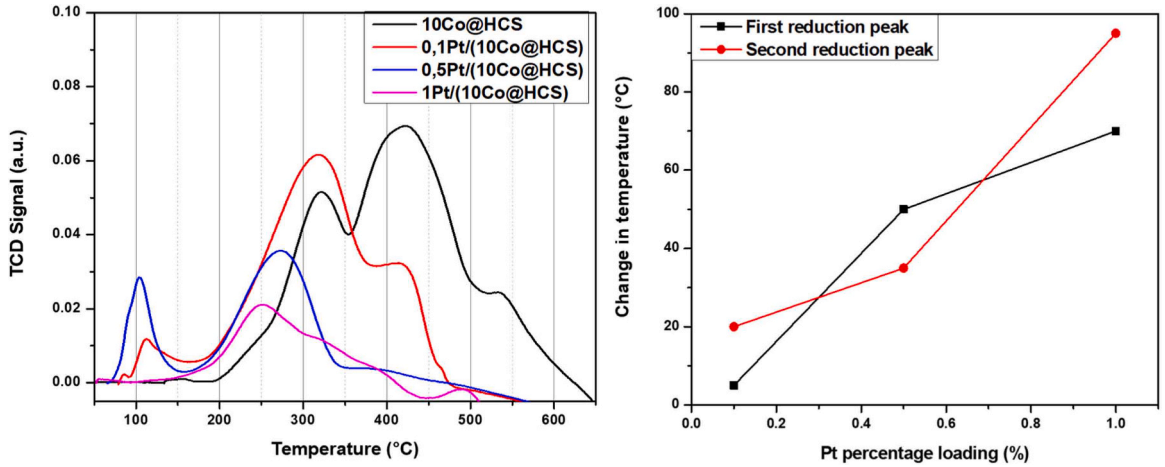

Fig. 5. (a) TPR profile of the primary hydrogen spillover effect and (b) the change in temperature with Pt percentage loading.

Table 3
The first and second reduction temperatures of the synthesised catalysts.

Sample	First Reduction Peak (°C)	Second Reduction Peak (°C)
10 %Co@ HCS	320	430
10Co0.1Pt@HCS	325	390
10Co0.5Pt@HCS	260	325
10Co1Pt@HCS	230	350
0.1Pt/(10Co@HCS)	315	410
0.5Pt/(10Co@HCS)	270	395
1Pt/(10Co@HCS)	250	335

Generally, one hydrogen molecule is consumed in the first reduction step of Co_3O_4 nanoparticles (Eq. 1), followed by consumption of three hydrogen molecules in the second reduction step (Eq. 2). A reduction peak ratio is thus expected to be 1:3 and such an observation is seen in the TPR profile of Co@HCS catalyst. However for the promoted catalysts the ratio is much smaller and this observation relates to some pre-reduction of the Co by the Pt and the carbon support [32].

From the reduction profiles observed it can be confirmed that Pt does facilitate both the primary and secondary hydrogen spillover effects. Additionally, it was found that the promoter effects of Pt were not as prominent when Co_3O_4 and Pt were separated by a carbon shell compared to when the two metals were in close proximity.

3.6. The effect of spillover

The spillover effect, particularly from Pt, Os and Ru promoters to the cobalt catalyst, influences the crystalline phase distribution of Co, specifically the hcp/fcc ratio (Table 5) and ultimately the catalytic performance. The Os and Ru data comes from published papers from our group where the promoters were characterized and analysed in FTS [51,78]. The observed changes in the hcp/fcc ratio can be attributed to the migration and interaction of Pt, Os and Ru species with the cobalt active sites.

Pt appears to be effective in promoting the formation of the Co(hcp) phase, with a notable increase in the hcp/fcc ratio with increasing Pt loading in CoxPt@HCS catalysts. However, the xPt/(10Co@HCS) (0.5 and 1 % loading Pt) catalysts which require a secondary spillover showed an hcp/fcc ratio of 0.60 and 0.52, respectively, suggesting a decrease in the hcp phase with increasing Pt loading.

In the case of the Ru promoter, the analysis was conducted in in-situ isothermal H_2 reduction at 450 °C temperature conditions [79]. While the H_2 reducing conditions are different to those used for the Pt-Co system, the Ru promoter was effective in the promotion of the Co(hcp) phase when the Ru and Co (CoxRu@HCS catalyst) were in direct contact versus when they were separated. The hcp/fcc ratio was exceedingly large when the Ru promoter was loaded inside (9.78) the NHCS compared to when loaded outside (0.71).

Studies on Os promoted Co phase for 10Co0.1Os@HCS, gave a hcp/fcc ratio of 0.13, indicating a low concentration of the hcp phase. Increasing the Os content gave an increase in the the hcp/fcc ratio (10Co0.5Os@HCS, 0.23, 10Co1Os@HCS, 1.33), In contrast xOs/(10Co@HCS) (0.1 and 0.5 % loading Os) catalysts showed only the presence of the Co fcc phase while the 1Os/(10Co@HCS) catalyst showed only the Co_3O_4 and CoO phases. Here, secondary spillover of an Os promoted Co catalyst did not favour the formation of the Co hcp phase.

In summary, the Pt and Ru generally exhibited a more significant promotion of the Co (hcp) phase compared to Os (Table 4). The primary spillover effect favoured the hcp phase formation for the Pt, Os and Ru promoted cobalt catalysts.

3.7. Fischer-Tropsch synthesis (FTS) evaluation

The FTS performance and promoter effect on the synthesised catalysts were evaluated at 220 (Table 5) and 250 °C (Table S3) for 50 h at each reaction temperature. Prior to FTS evaluation, a pre-treatment in-situ hydrogen reduction of the catalysts was performed at a temperature of 350 °C for 18 h [50,80,81]. FTS CO conversion and selectivity data were then obtained for 10Co@HCS, 10CoPtx@HCS and Ptx/(10Co@HCS) catalysts as shown in Table 5.

From the table the catalytic activities of the catalysts followed the following order 10Co1Pt@HCS (15.0 %) > 1Pt/(10Co@HCS) (6.7 %)

Table 4
Catalysts relative Co phase abundance (wt%).

Sample	Co(Fcc)	Co(Hcp)	Hcp/Fcc Ratio
10 %Co@HCS	-	-	-
10Co0.1Os@HCS	37.10	4.68	0.13
10Co0.Os@HCS	81.35	18.65	0.23
10Co1Os@HCS	43	57	1.33
0.1 %Os/(Co@HCS)	100	-	-
0.5 %Os/(Co@HCS)	63.74	-	-
1 %Os/(Co@HCS)	-	-	-
10Co0.1Pt@HCS	30.96	5.81	0.19
10Co0.5Pt@HCS	35.92	8.21	0.23
10Co1Pt@HCS	39.21	29.43	0.75
[a]10Co0.5Ru@NHCS	9	88	9.78
0.1Pt/Co@HCS	-	-	-
0.5Pt/(10Co@HCS)	20.78	12.49	0.60
1Pt/(10Co@HCS)	31.18	16.09	0.52
[a]0.5Ru/(10Co@NHCS)	58	41	0.71

[a] PXRD patterns of Co catalysts encapsulated in nitrogen-doped HCS, reduced in 50 %H_2 gas at 450 °C for 3 hours [79].

Table 5
Fischer-Tropsch synthesis performance of the catalysts.

Sample	CO Conversion (%)	TOF (x10^{-3} s)[a]	Activity (x10^{-6}) (mol_{CO}/g_{Co}.s)	Selectivity (C mol) %		
				C_1	C_2-C_4	C_{5+}
10Co@HCS	4,2	6	27,8	18.8	11.1	70.1
0.1 %PtCo@HCS	11,3	6,1	42,1	24.6	12.3	63.1
0.5 %PtCo@HCS	13,3	10.0	52,8	26.8	11.7	61.5
1 %PtCo@HCS	15	18.0	59,6	31.3	12.4	56.3
0.1 %Pt/(Co@HCS)	5,1	3,9	20,6	20.8	8.3	70.9
0.5 %Pt/(Co@HCS)	6	6,9	24,8	21.6	8.8	69.6
1 %Pt/(Co@HCS)	6,7	9,9	33.0	22.5	9.2	68.3

[a] TOF $= \frac{-r_{c0}.N_{av}}{S}$ where N_{av} is Avogadro's number and S is the number of active sites.

>10Co@HCS (4.2 %). This trend was found at both reaction temperatures. As the temperature rose, as expected, the CO conversion increased for all of the catalysts. The unpromoted catalyst was shown to have the lowest CO conversion compared to the Pt promoted catalysts, thus showing that both primary and secondary spillover effects resulted in increased CO conversions [82]. A significant increase in CO conversion was observed when the intimacy between the Co and Pt promoter was increased. Due to the direct contact or close proximity of Pt with Co, easy reduction of the Co oxide was expected which subsequently resulted in the generation of active Co(hcp) particles [12]. The active Co (hcp) phase has a higher intrinsic activity for CO hydrogenation reactions compared to the Co(fcc) phase [38].

It is worth noting that promoters, such as Pt, can also have a "cleansing effect" on the Co surface by removing unreactive species such as carbon, which can enhance the CO conversion [35,83,84]. This effect is likely to be more pronounced when Co and Pt are in close contact, as was observed with CoPt@HCS catalysts.

The Pt/(Co@HCS) catalysts showed lower activity than the CoPt@HCS catalyst. This could be due to the distance that the spillover hydrogen has to travel (~30 nm) [24,78]. Additionally, the carbon shell separating the Co and Pt may block some of the pores of the support, limiting the diffusion of the spillover H atoms which was observed in the BET studies.

A diminished Pt promoter effect in the secondary hydrogen spillover process was also observed by Nabaho et al. for their catalyst, where Pt and Co were separated on an alumina support [83]. They attributed this effect to CO poisoning of the Pt surface, which can inhibit the hydrogenation reaction [85]. This phenomenon is well-known in olefin hydrogenation reactions and in PEM fuel cells [86].

The locations of the Co and Pt were also observed to affect the hydrocarbon selectivity of the catalysts. Thus, the methane selectivity increased with increased contact between Pt and Co: 10 %Co@HCS (18.8 %) < 1Pt/(10Co@HCS) (22.5 %) < 10Co1Pt@HCS (31.3 %). Another observation was that an increase in Pt loading resulted in increased methane selectivity and a decrease in C_5+ liquid hydrocarbons. A high selectivity for the production of high molecular weight hydrocarbons was demonstrated by the unpromoted catalyst, C_5+, compared to the Pt promoted Co catalysts and this is likely due to the high hydrogenation activity of the Pt promoter, which is generally expected in catalysts with Pt loadings greater than 0.1 % [87]. The close contact between Co and Pt in the CoPt@HCS catalyst resulted in a higher methane selectivity [88].

Overall, the catalytic activity and selectivity of the Co catalyst were both impacted by the varied locations of the Pt and Co nanoparticles in FTS.

4. Conclusion

In conclusion, several Co-based catalysts were successfully synthesized, including Co@HCS, CoPt@HCS and Pt/(Co@HCS). EDX spectra confirmed the presence of the Co and Pt nanoparticles in the catalysts.

The catalysts were evaluated using various techniques, including TPR, in-situ XRD, and FT performance, and the results showed that Pt has a positive effect on the Co catalysts, enhancing their reducibility and improving their performance in CO conversion and hydrocarbon selectivity. The primary hydrogen spillover effect was found to make a significant contribution in reducing Co_3O_4 to metallic active phase Co^0, while the secondary hydrogen spillover effect had a lesser effect, possibly due to the carbon shell (~28 nm) distance between Pt and Co and the limitations of hydrogen atom gas and surface diffusion. A higher Co (hcp) to Co (fcc) ratio was achieved from the reduction of the Co_3O, when Pt and Co were in intimate contact. As a result, the highest degree of CO conversion was observed for CoPt@HCS (FT data) and the hydrocarbon selectivity also showed that the primary hydrogen spillover effect increased methane production which was undesirable.

Overall, these findings confirms that Pt can be effectively used as a promoter for Co oxide catalysts, and further, that the distance between Pt and Co plays a role in the efficiency of the hydrogen spillover effect.

Author contributions

The manuscript was written through the contributions of all authors. All authors have approved the final version of the manuscript.

CRediT authorship contribution statement

Roy Forbes: Writing – review & editing, Validation, Software, Formal analysis. **Neil John Coville:** Writing – review & editing, Project administration, Funding acquisition, Conceptualization. **Tshepo Molefe:** Writing – review & editing, Writing – original draft, Visualization, Software, Methodology, Investigation, Formal analysis, Data curation, Conceptualization. **Joy Masilo-Kumi:** Writing – review & editing, Resources, Investigation.

Declaration of Competing Interest

We wish to confirm that there are no known conflicts of interest associated with this publication.

All of the sources of funding for the work described in this publication are acknowledged in the article to be published.

We agree that the submission of an article implies that the work described has not been published previously, that it is not under consideration for publication elsewhere, that its publication is approved by all authors and tacitly or explicitly by the responsible authorities where the work was carried out, and that, if accepted, it will not be published elsewhere in the same form, in English or in any other language, including electronically without the written consent of the copyright-holder.

We confirm that the manuscript has been read and approved by all named authors.

We confirm that the order of authors listed in the manuscript has been approved by all named authors.

Data availability

Data will be made available on request.

Acknowledgements

We wish to thank the University of the Witwatersrand, the NRF and the DSI-NRF Centre of Excellence in Catalysis for financial support.

Appendix A. Supporting information

Supplementary data associated with this article can be found in the online version at doi:10.1016/j.apcata.2024.119863.

References

[1] E. Iglesia, S.C. Reyes, R.J. Madon, S.L. Soled, Selectivity control and catalyst design in the Fischer-Tropsch synthesis: sites, pellets, and reactors, Adv. Catal. 39 (1993) 221–302.
[2] A.Y. Khodakov, W. Chu, P. Fongarland, Advances in the development of novel cobalt Fischer-Tropsch catalysts for synthesis of long-chain hydrocarbons and clean fuels, Chem. Rev. 107 (2007) 1692–1744, https://doi.org/10.1021/cr050972v.
[3] Bahome M.C. (2007) Synthesis and use of carbon nanotubes as a support for the Fischer-Tropsch Synthesis.
[4] K. Snavely, B. Subramaniam, On-Line gas chromatographic analysis of Fischer–Tropsch synthesis products formed in a supercritical reaction medium, Ind. Eng. Chem. Res 36 (1997) 4413–4420.
[5] L. Cheng, Q. Xiang, Y. Liao, H. Zhang, CdS-based photocatalysts, Energy Environ. Sci. 11 (2018) 1362–1391.
[6] G. Yilmaz, S.B. Peh, D. Zhao, G.W. Ho, Atomic-and molecular-level design of functional metal–organic frameworks (MOFs) and derivatives for energy and environmental applications, Adv. Sci. 6 (2019) 1901129.
[7] M.F. Rojas-Michaga, S. Michailos, E. Cardozo, et al., Sustainable aviation fuel (SAF) production through power-to-liquid (PtL): a combined techno-economic and life cycle assessment, Energy Convers. Manag 292 (2023) 117427.
[8] A.K. Dalai, B.H. Davis, Fischer–Tropsch synthesis: a review of water effects on the performances of unsupported and supported Co catalysts, Appl. Catal. A Gen. 348 (2008) 1–15.
[9] A.Y. Khodakov, A. Griboval-Constant, R. Bechara, F. Villain, Pore-size control of cobalt dispersion and reducibility in mesoporous silicas, J. Phys. Chem. B 105 (2001) 9805–9811.
[10] C.J. Bertole, C.A. Mims, G. Kiss, Support and rhenium effects on the intrinsic site activity and methane selectivity of cobalt Fischer–Tropsch catalysts, J. Catal. 221 (2004) 191–203.
[11] V. Subramanian, K. Cheng, C. Lancelot, et al., Nanoreactors: an efficient tool to control the chain-length distribution in fischer-tropsch synthesis, ACS Catal. 6 (2016) 1785–1792, https://doi.org/10.1021/acscatal.5b01596.
[12] S. Lyu, L. Wang, J. Zhang, et al., Role of active phase in Fischer–Tropsch synthesis: experimental evidence of CO activation over single-phase cobalt catalysts, ACS Catal. 8 (2018) 7787–7798.
[13] E. Iglesia, D. Hibbitts, The Fischer–Tropsch synthesis: a few enduring mechanistic conundrums revisited, J. Catal. 405 (2022) 614–625.
[14] I.C. ten Have, B.M. Weckhuysen, The active phase in cobalt-based Fischer-Tropsch synthesis, Chem. Catal. 1 (2021) 339–363.
[15] W. Chu, P.A. Chernavskii, L. Gengembre, et al., Cobalt species in promoted cobalt alumina-supported Fischer–Tropsch catalysts, J. Catal. 252 (2007) 215–230.
[16] Y. Zhang, Y. Yoneyama, K. Fujimoto, N. Tsubaki, A new preparation method of bimodal catalyst support and its application in Fischer–Tropsch synthesis, Top. Catal. 26 (2003) 129–137.
[17] M. Voß, D. Borgmann, G. Wedler, Characterization of alumina, silica, and titania supported cobalt catalysts, J. Catal. 212 (2002) 10–21.
[18] L. Spadaro, F. Arena, M.L. Granados, et al., Metal–support interactions and reactivity of Co/CeO2 catalysts in the Fischer–Tropsch synthesis reaction, J. Catal. 234 (2005) 451–462.
[19] E. Iglesia, S.L. Soled, R.A. Fiato, Fischer-Tropsch synthesis on cobalt and ruthenium. Metal dispersion and support effects on reaction rate and selectivity, J. Catal. 137 (1992) 212–224.
[20] T.N. Phaahlamohlaka, D.O. Kumi, M.W. Dlamini, et al., Ruthenium nanoparticles encapsulated inside porous hollow carbon spheres: a novel catalyst for Fischer–Tropsch synthesis, Catal. Today 275 (2016) 76–83, https://doi.org/10.1016/j.cattod.2015.11.034.
[21] R.P. Nippes, P.D. Macruz, M.H.N.O. Scaliante, L. Cardozo-Filho, Fischer–Tropsch synthesis using cobalt catalysts supported on graphene materials: a systematic review, Res Chem. Inter. 49 (2023) 2025–2052.
[22] A.C. Ghogia, A. Nzihou, P. Serp, et al., Cobalt catalysts on carbon-based materials for Fischer-Tropsch synthesis: a review, Appl. Catal. A Gen. 609 (2021) 117906.
[23] R. Liu, F. Qu, Y. Guo, et al., Au@ carbon yolk–shell nanostructures via one-step core–shell–shell template, Chem. Commun. 50 (2014) 478–480.
[24] I. Nongwe, G. Bepete, A. Shaikjee, et al., Synthesis of gold encapsulated in spherical carbon capsules with a mesoporous shell structure. A robust catalyst in a nanoreactor, Catal. Commun. 53 (2014) 77–82.
[25] S. Li, J. Niu, Y.C. Zhao, et al., High-rate aluminium yolk-shell nanoparticle anode for Li-ion battery with long cycle life and ultrahigh capacity, Nat. Commun. 6 (1) (2015) 7.
[26] X. Fang, J. Zang, X. Wang, et al., A multiple coating route to hollow carbon spheres with foam-like shells and their applications in supercapacitor and confined catalysis, J. Mater. Chem. A 2 (2014) 6191–6197.
[27] Z.-A. Qiao, B. Guo, A.J. Binder, et al., Controlled synthesis of mesoporous carbon nanostructures via a "silica-assisted" strategy, Nano Lett. 13 (2013) 207–212.
[28] G. He, S. Evers, X. Liang, et al., Tailoring porosity in carbon nanospheres for lithium–sulfur battery cathodes, ACS Nano 7 (2013) 10920–10930.
[29] G.-H. Wang, J. Hilgert, F.H. Richter, et al., Platinum–cobalt bimetallic nanoparticles in hollow carbon nanospheres for hydrogenolysis of 5-hydroxymethylfurfural, Nat. Mater. 13 (2014) 293–300.
[30] H. Xiong, M.A.M. Motchelaho, M. Moyo, et al., Cobalt catalysts supported on a micro-coil carbon in Fischer–Tropsch synthesis: a comparison with CNTs and CNFs, Catal. Today 214 (2013) 50–60.
[31] M. Trepanier, A.K. Dalai, N. Abatzoglou, Synthesis of CNT-supported cobalt nanoparticle size on reducibility, activity and selectivity in Fischer-Tropsch reactions, Appl. Catal. A Gen. 374 (2010) 79–86.
[32] J. Hong, E. Marceau, A.Y. Khodakov, et al., Speciation of ruthenium as a reduction promoter of silica-supported Co catalysts: a time-resolved in situ XAS investigation, ACS Catal. 5 (2015) 1273–1282.
[33] J. Horáček, Fischer–Tropsch synthesis, the effect of promoters, catalyst support, and reaction conditions selection, Mon. F. üR. Chem. -Chem. Mon. 151 (2020) 649–675.
[34] G. Jacobs, T.K. Das, Y. Zhang, et al., Fischer-Tropsch synthesis: support, loading, and promoter effects on the reducibility of cobalt catalysts, Appl. Catal. A Gen. 233 (2002) 263–281, https://doi.org/10.1016/S0926-860X(02)00195-3.
[35] S.K. Beaumont, S. Alayoglu, C. Specht, et al., Combining in situ NEXAFS spectroscopy and CO2methanation kinetics to study Pt and Co nanoparticle catalysts reveals key insights into the role of platinum in promoted cobalt catalysis, J. Am. Chem. Soc. 136 (2014) 9898–9901, https://doi.org/10.1021/ja505286j.
[36] A. Panda, E. Kim, Y.N. Choi, et al., Phase controlled synthesis of Pt doped co nanoparticle composites using a metal-organic framework for Fischer–Tropsch catalysis, Catalysts 9 (2019) 156.
[37] Z. Gholami, Z. Tišler, V. Rubáš, Recent advances in Fischer-Tropsch synthesis using cobalt-based catalysts: a review on supports, promoters, and reactors, Catal. Rev. 63 (2021) 512–595.
[38] S.K. Beaumont, S. Alayoglu, C. Specht, et al., A nanoscale demonstration of hydrogen atom spillover and surface diffusion across silica using the kinetics of CO2 methanation catalyzed on spatially separate Pt and Co nanoparticles, Nano Lett. 14 (2014) 4792–4796.
[39] W.C. Conner Jr, J.L. Falconer, Spillover in heterogeneous catalysis, Chem. Rev. 95 (1995) 759–788.
[40] Nabaho D. (2015) Hydrogen spillover in the Fischer-Tropsch synthesis: the role of platinum and gold as promoters in cobalt-based catalysts.
[41] S. Khoobiar, Particle to particle migration of hydrogen atoms on platinum—alumina catalysts from particle to neighboring particles, J. Phys. Chem. 68 (1964) 411–412.
[42] W. Karim, C. Spreafico, A. Kleibert, et al., Catalyst support effects on hydrogen spillover, Nature 541 (2017) 68–71.
[43] A.J. Lachawiec, G. Qi, R.T. Yang, Hydrogen storage in nanostructured carbons by spillover: bridge-building enhancement, Langmuir 21 (2005) 11418–11424.
[44] S.J. Teichner, The history and perspectives of spillover. Studies in Surface Science and Catalysis, Elsevier, 1993, pp. 27–43.
[45] A. Lueking, R.T. Yang, Hydrogen spillover from a metal oxide catalyst onto carbon nanotubes—implications for hydrogen storage, J. Catal. 206 (2002) 165–168.
[46] M. Hirscher, M. Becher, Hydrogen storage in carbon nanotubes, J. Nanosci. Nanotechnol. 3 (2003) 3–17.
[47] Y.-Y. Liu, J.-L. Zeng, J. Zhang, et al., Improved hydrogen storage in the modified metal-organic frameworks by hydrogen spillover effect, Int J. Hydrog. Energy 32 (2007) 4005–4010.
[48] V.V. Rozanov, O.V. Krylov, Hydrogen spillover in heterogeneous catalysis, Russ. Chem. Rev. 66 (1997) 107.
[49] R. Prins, Hydrogen spillover. Facts and fiction, Chem. Rev. 112 (2012) 2714–2738.
[50] T.N. Phaahlamohlaka, D.O. Kumi, M.W. Dlamini, et al., Effects of Co and Ru intimacy in Fischer–Tropsch catalysts using hollow carbon sphere supports: assessment of the hydrogen spillover processes, ACS Catal. 7 (2017) 1568–1578.
[51] Molefe T., Barrett D., Diaz B., et al (2023) Fischer-Tropsch synthesis: osmium promoted Co@ HCS catalysts. J Catal.
[52] P. Mente, T.N. Phaahlamohlaka, V. Mashindi, N.J. Coville, Polystyrene-b-poly (acrylic acid) nanospheres for the synthesis of size-controlled cobalt nanoparticles encapsulated inside hollow carbon spheres, J. Mater. Sci. 56 (2021) 2113–2128.
[53] R. Mohamed, T. Binninger, P.J. Kooyman, et al., Facile deposition of Pt nanoparticles on Sb-doped SnO 2 support with outstanding active surface area for the oxygen reduction reaction, Catal. Sci. Technol. 8 (2018) 2672–2685.
[54] J. Fu, Q. Xu, J. Chen, et al., Controlled fabrication of uniform hollow core porous shell carbon spheres by the pyrolysis of core/shell polystyrene/cross-linked polyphosphazene composites, Chem. Commun. 46 (2010) 6563–6565.
[55] G. Qi, Y. Wang, L. Estevez, et al., Facile and scalable synthesis of monodispersed spherical capsules with a mesoporous shell, Chem. Mater. 22 (2010) 2693–2695.
[56] N. Li, Q. Zhang, J. Liu, et al., Sol–gel coating of inorganic nanostructures with resorcinol–formaldehyde resin, Chem. Commun. 49 (2013) 5135–5137.
[57] X. Fang, S. Liu, J. Zang, et al., Precisely controlled resorcinol–formaldehyde resin coating for fabricating core–shell, hollow, and yolk–shell carbon nanostructures, Nanoscale 5 (2013) 6908–6916.

[58] S. Li, A. Pasc, V. Fierro, A. Celzard, Hollow carbon spheres, synthesis and applications–a review, J. Mater. Chem. A 4 (2016) 12686–12713.
[59] M. Zheng, J. Cao, X. Chang, et al., Preparation of oxide hollow spheres by colloidal carbon spheres, Mater. Lett. 60 (2006) 2991–2993.
[60] W. Stober, A. Fink, Controlled growth of monodispersed silica spheres in the micron size range, J. Colloid Interface Sci. 26 (1968) 62–69, https://doi.org/10.1016/0021-9797(68)90272-5.
[61] N.D. Petkovich, A. Stein, Controlling macro-and mesostructures with hierarchical porosity through combined hard and soft templating, Chem. Soc. Rev. 42 (2013) 3721–3739.
[62] H. Zhang, W. Chu, C. Zou, et al., Promotion effects of platinum and ruthenium on carbon nanotube supported cobalt catalysts for Fischer–Tropsch synthesis, Catal. Lett. 141 (2011) 438–444.
[63] J.-S. Girardon, A.S. Lermontov, L. Gengembre, et al., Effect of cobalt precursor and pretreatment conditions on the structure and catalytic performance of cobalt silica-supported Fischer–Tropsch catalysts. J. Catal. 230 (2005) 339–352.
[64] Masilo J. (2019) Investigation of the hydrogen spillover effect in platinum promoted cobalt/hollow carbon spheres.
[65] X. Chen, K. Kierzek, K. Cendrowski, et al., CVD generated mesoporous hollow carbon spheres as supercapacitors, Colloids Surf. A Physicochem Eng. Asp. 396 (2012) 246–250.
[66] W. Chen, X. Pan, M.-G. Willinger, et al., Facile autoreduction of iron oxide/carbon nanotube encapsulates, J. Am. Chem. Soc. 128 (2006) 3136–3137.
[67] Tropsch F., Panda A., Kim E., et al (2019) Phase Controlled Synthesis of Pt Doped Co Nanoparticle Composites Using a Metal-Organic. https://doi.org/10.3390/catal9020156.
[68] L.A. Bruce, M. Hoang, A.E. Hughes, T.W. Turney, Ruthenium promotion of Fischer-Tropsch synthesis over coprecipitated cobalt/ceria catalysts, Appl. Catal. A Gen. 100 (1993) 51–67.
[69] S.J. Gregg, K.S.W. Sing, H.W. Salzberg, Adsorption surface area and porosity, J. Electrochem Soc. 114 (1967) 279C.
[70] C. Galeano, R. Güttel, M. Paul, et al., Yolk-shell gold nanoparticles as model materials for support-effect studies in heterogeneous catalysis: Au, @C and Au, @ZrO2 for CO oxidation as an example, Chem. - A Eur. J. 17 (2011) 8434–8439, https://doi.org/10.1002/chem.201100318.
[71] X. Chen, K. Kierzek, K. Wenelska, et al., Electrochemical characteristics of discrete, uniform, and monodispersed hollow mesoporous carbon spheres in double-layered supercapacitors, Chem. Asian J. 8 (2013) 2627–2633.
[72] J. Van de Loosdrecht, S. Barradas, E.A. Caricato, et al., Calcination of Co-based Fischer–Tropsch synthesis catalysts, Top. Catal. 26 (2003) 121–127.
[73] M.P. Rosynek, C.A. Polansky, Effect of cobalt source on the reduction properties of silica-supported cobalt catalysts, Appl. Catal. 73 (1991) 97–112.
[74] D. Nabaho, J.W.H. Niemantsverdriet, M. Claeys, E. van Steen, Hydrogen spillover in the Fischer–Tropsch synthesis: an analysis of gold as a promoter for cobalt–alumina catalysts, Catal. Today 275 (2016) 27–34.
[75] Schanke D., Vada S., Blekkan E.A., et al (1996) Study of Pt-promoted cobalt CO hydrogenation catalysts.
[76] D. Nabaho, J.W.H. Niemantsverdriet, M. Claeys, E. van Steen, Hydrogen spillover in the Fischer–Tropsch synthesis: an analysis of platinum as a promoter for cobalt–alumina catalysts, Catal. Today 261 (2016) 17–27.
[77] A.M. Hilmen, D. Schanke, A. Holmen, TPR study of the mechanism of rhenium promotion of alumina-supported cobalt Fischer-Tropsch catalysts, Catal. Lett. 38 (1996) 143–147.
[78] T.N. Phaahlamohlaka, D.O. Kumi, M.W. Dlamini, et al., Effects of Co and Ru intimacy in Fischer-Tropsch catalysts using hollow carbon sphere supports: assessment of the hydrogen spillover processes, ACS Catal. 7 (2017) 1568–1578, https://doi.org/10.1021/acscatal.6b03102.
[79] Buthelezi T.I. (2019) Carbon with different functionalities as a hydrogen transport layer in ruthenium promoted Fischer-Tropsch catalysts.
[80] G.L. Bezemer, P.B. Radstake, U. Falke, et al., Investigation of promoter effects of manganese oxide on carbon nanofiber-supported cobalt catalysts for Fischer–Tropsch synthesis, J. Catal. 237 (2006) 152–161.
[81] X. Xu, H. Oosterbeek, J.H. Bitter, et al., Cobalt particle size effects in the fischer−tropsch reaction studied with carbon nanofiber supported catalysts, J. Am. Chem. Soc. 128 (2006) 3956–3964, https://doi.org/10.1021/ja058282w.
[82] A. Kogelbauer, J.G. Goodwin Jr, R. Oukaci, Ruthenium promotion of Co/Al2O3Fischer–Tropsch catalysts, J. Catal. 160 (1996) 125–133.
[83] D. Nabaho, J.W.H. Niemantsverdriet, M. Claeys, E. Steen, Van, Hydrogen spillover in the Fischer – Tropsch synthesis: an analysis of platinum as a promoter for cobalt – alumina catalysts, Catal. Today 261 (2016) 17–27, https://doi.org/10.1016/j.cattod.2015.08.050.
[84] E. Iglesia, S.L. Soled, R.A. Fiato, G.H. Via, Bimetallic synergy in cobalt ruthenium Fischer-Tropsch synthesis catalysts, J. Catal. 143 (1993) 345–368.
[85] K.S. Hwang, M. Yang, J. Zhu, et al., The molecular mechanism of the poisoning of platinum and rhodium catalyzed ethylene hydrogenation by carbon monoxide, J. Mol. Catal. A Chem. 204 (2003) 499–507.
[86] J.J. Baschuk, X. Li, Carbon monoxide poisoning of proton exchange membrane fuel cells, Int J. Energy Res 25 (2001) 695–713.
[87] F. Diehl, A.Y. Khodakov, Promotion of cobalt Fischer-Tropsch catalysts with noble metals: a review, Oil Gas. Sci. Technol. l'IFP 64 (2009) 11–24.
[88] W. Ma, G. Jacobs, R. Keogh, et al., Fischer-Tropsch synthesis: Effect of Pt promoter on activity, selectivities to hydrocarbons and oxygenates, and kinetic parameters over 15% Co/Al2O3. Synthetic Liquids Production and Refining, ACS Publications, 2011, pp. 127–153.